1 **Characterization and prediction of tropical cyclone forerunner surge**

2 **Yi Liu[1], Jennifer L. Irish[1]**

3 [1]Department of Civil and Environmental Engineering, Virginia Tech, Blacksburg, VA, USA

4 Corresponding author: Yi Liu (echoliu@vt.edu)

5 **Highlights:**

6 • Physical scaling laws are revealed to characterize forerunner surge from storm track

7 parameters (central pressure, radius, and speed).

8 • The physical scaling enables rapid forecasting of forerunner surge.

9 **Abstract**

10 Forerunner surge, a water level rise ahead of tropical cyclone landfall, often strikes

11 coastal communities unexpectedly, stranding people and increasing loss of life. Surge forecasting

12 systems and emergency managers almost exclusively focus on peak surge, while much less

13 attention is given to forerunner surge. To address the need for fast and accurate forecasting of

14 forerunner surge, we analyze high-fidelity surge simulations in Virginia, New York/New Jersey

15 and Texas and extract physical scaling laws between readily available storm track information

16 and forerunner surge magnitude and timing. We demonstrate that a dimensionless relationship

17 between central-pressure scaled surge and wind-duration scaled time may effectively be used for

18 rapid forerunner surge forecasting, where uncertainty is considered. We use our method to

19 predict forerunner surge for Hurricanes Ike (2008)—a significant forerunner surge event—and

20 Harvey (2017). The predicted forerunner surge 24 to 6 hours before Hurricane Ike's landfall

21 ranged from 0.4 to 2.8 m, where the observed forerunner surge ranged from 0.4 to 2.6 m. This

22   new method has the potential to be incorporated into real-time surge forecasting systems to aid

23   emergency management and evacuation decisions.

24   Keywords: Tropical cyclones; forerunner surge; modeling; forecasting; physical scaling;

25   ADCIRC.

26

1 Introduction

Tropical cyclone (TC) storm surge has had devastating impacts on coastal communities worldwide, causing tremendous loss of life and physical damage. Peak surge is most often the dominant driver of direct damage. Consequently, surge forecasting systems and emergency managers have focused on improving prediction of peak surge, while less attention has been given to forecasting forerunner surge—a storm-induced early water level rise above mean sea level well in advance of TC landfall. The significance of forerunner surge was first observed in 1900, when Galveston, Texas was hit by a forerunner surge of 1.5 m 12 hours prior to landfall [1,2]. This forerunner surge flooded essential roadways and stranded many people on Galveston Island, directly contributing to the shocking death of 8,000 people, and making the 1900 Galveston Hurricane the deadliest hurricane on record [3]. Forerunner surge is most dangerous for those who are in the direct path of the cyclone, where the forerunner surge precedes a high peak surge. Significant forerunner surges occurred in 1900 and again in 2008 (Hurricane Ike) when these storms made landfall in Galveston. Since 1900, forerunner surge on the order of 1 to 2 m has been documented for TCs impacting both the US Gulf of Mexico and Atlantic coasts (Table 1). Yet, while a few studies indicated that large TCs making landfall across a broad, shallow continental shelf could potentially generate significant forerunner surges [2,4]—where Kennedy et al. demonstrated Hurricane Ike's large forerunner surge was predominantly from Ekman setup (water level rise arising from the influence of Coriolis force)—we lack a basic quantitative understanding of how and when significant forerunner surge is generated.

To better inform evacuation plans and thereby reduce loss of life, it is important to understand the conditions in which a TC generates significant forerunner surge. Surge forecasts historically focus on the rapid and accurate prediction of peak surge, and due to the need for

50   rapid forecasting, either use a large ensemble set of track possibilities with low-fidelity surge

51   simulations (e.g., NOAA's P-Surge [5,6]), use a small, discrete set of storm track possibilities

52   with high-fidelity surge simulations (e.g., [7]), or use interpolation schemes to determine peak

53   surge from discrete, high-fidelity simulations for a large ensemble of track possibilities (e.g.,

54   [8,9]). Some rapid surge prediction methods also consider forecasting of surge time series, where

55   either accuracy was compromised [7] or interpolation schemes were used [10]. Forerunner surge

56   is often overlooked when considering real-time forecasts.

57   Herein, to advance the physical understanding of forerunner surge generation and provide

58   a reliable and rapid forerunner surge forecasting method, we examine time series from high-

59   fidelity storm surge simulations for Galveston, TX, Hampton Roads, VA, and New York/New

60   Jersey, and we characterize forerunner surge magnitude and timing using physical scaling laws

61   based on storm track parameters.

62   **2 Methods**

63   The forerunner surge observational record is sparse, both in terms of the number of

64   cyclones observed and in spatiotemporal coverage, so we base our analysis on simulated wind,

65   barometric pressure, and surge for a range of synthetic TCs representative of observed storm

66   characteristics [11]. Here, the unstructured finite-element shallow water equations code ADCIRC

67   [12] is used, coupled with a spectral wave model (e.g., SWAN [13] or STWAVE [14]) to include

68   the effects of wave setup [15,16]. Runup from individual waves is not included. TC wind and

69   pressure fields are generated from a planetary boundary layer (PBL) model [17], using storm

70   track parameters as input, including storm position, central pressure deficit (Δp) representing

71   intensity, radii to maximum wind (R) representing storm size, forward speed (V_f), heading (θ),

72   and profile parameter Holland B [18]. Our focus herein is on characterizing the forerunner surge

73 anomaly (level above expected normal level). To simplify the analysis, astronomical tides are not

74 considered.

75   We conduct dimensional analysis on the simulations to find physical scaling laws relating

76 surge timing and magnitude to storm track parameters 12 to 24 hours before landfall. Former

77 studies have shown that the storm parameters most influencing the magnitude of peak surge are

78 landfall location (x_o), Δp, and R, while V_f and θ have less impact [19]. In this forerunner surge

79 study we also focus on the storm parameters Δp and R. However, we identify through sensitivity

80 analyses that V_f also significantly influences forerunner surge, while heading and landfall

81 location have less impact. Specifically, while landfall location (x_0) is known to strongly

82 influence peak surge [20], our sensitivity analysis indicates forerunner surge (represented by

83 surge 12 hours before landfall) is not very sensitive to moderate shifts in track, especially at the

84 open coast. At location TX-2 in Figure 1, as an example, our simulations exhibit differences in

85 forerunner surge magnitude 12 hours before landfall of less than 0.1 m, when track spacing is

86 varied up to 35 km, and when all other storm parameters are held constant. Field observations

87 also support this conclusion (see Appendix A, Figures A2-A7). When track is varied up to 200

88 km to the south of Houston/Galveston (Figure A1), forerunner surge is generated, but its

89 magnitude does not change significantly, less than 0.2 m. Storms tracking 100 km or more to the

90 north, northeast of Houston/Galveston do not generate forerunner surge; Houston/Galveston is

91 well to the left of the hurricane eyewall for these storms, which thus result in strong offshore

92 winds in the study area. A sensitivity test is also conducted in terms of storm heading $(\theta,)$ and

93 results show little difference between storms with different headings (less than 0.1 m increase

94 over a heading change of ± 45 degrees at location TX-2), although results in the bay can be more

95 complicated due to locally generated surge—a process not directly considered herein.

96   Thus, for each region we consider just one heading, a limited range of x_o (where

97   forerunner surge precedes a peak along-coast surge occurring near the study location), and a

98   wide range of $\Delta p, R$ and V_f.

99   We leverage existing surge simulations for Virginia and New York/New Jersey and

100   perform our own simulations for Texas. In Virginia and New York/New Jersey, we use the US

101   Army Corps of Engineers (USACE) STWAVE+ADCIRC simulations [21]. For this study, 19

102   synthetic TCs along three tracks making landfall in or near Hampton Roads are selected (Figure

103   1). All storms follow headings of -60º clockwise from north. Track parameters Δp, R, and V_f are

104   respectively varied from 38 to 88 hPa, 25 to 109 km, and 3.3 to 12.2 m/s at landfall. Results are

105   shown for two representative locations near densely populated areas: Sewells Point (VA-1)

106   within Chesapeake Bay and Virginia Beach (VA-2) on the open coast. Similarly, 18 synthetic

107   TCs along three tracks in or near Sandy Hook, NJ are selected, with headings of -60o and track

108   parameters Δp, R, and Vf varying from 28 to 78 hPa, 31 to 139 km, and 6.7 to 18.6 m/s at

109   landfall. Results are shown for two representative locations near densely populated areas: The

110   Battery, NY (NJ-1) and Sandy Hook, NJ (NJ-2).

111   In Texas, we simulate surge using SWAN+ADCIRC, employing Dietrich et al.'s [16]

112   validated high-resolution computational mesh and model setup used in Kennedy et al.'s [2]

113   forerunner surge study. We first assess model performance using a synthetic TC similar to

114   Hurricane Ike in terms of these track parameters: Δp of 63 hPa, R of 74 km, and V_f of 18 km/h at

115   landfall [4,22]. Wind and pressure forcing are developed using the PBL model. It should also be

116   noted that herein we define the forerunner surge generally as the water level rise ahead of TC

117   landfall, for the purposes of this paper the surge time series during the period from 24 to 6 hours

118   prior to landfall. With this definition, the forerunner surge encompasses Ekman setup as well as

119   other processes inducing surge prior to landfall. This simulation is compared both with Kennedy

120   et al.'s [2] observations and simulation using the best available observation-based H*Wind wind

121   field (Figure 2). Some differences exist between observations and our model results using

122   parameterized wind forcing, and most of these cannot be eliminated, even when using the

123   observation-based H*Wind forcing. Repeating Kennedy et al.'s analysis, our surge simulation

124   using parameterized winds when Coriolis force is disabled shows that the major part of Ike's

125   forerunner surge indeed does arise from Ekman setup, and is captured when using the

126   parameterized wind field. Note that the simulated surge time series herein do not show a

127   forerunner peak that is observed during Hurricane Ike, and we think this arises for two reasons.

128   First, although using a best wind field hindcast will certainly provide a more accurate simulated

129   estimate with a forerunner peak, we purposefully elect to use parameterized wind fields because

130   we want our results to be useful for forecasting purposes. Second, we hypothesize that the depth-

131   averaged model underestimates the current speed of importance to forerunner surge (that in the

132   upper ocean layer), thus underestimating the forerunner peak. This underestimate is also see in

133   the simulations using H*Wind. Thus, although exhibiting some error, the synthetic storm surge

134   simulations analyzed herein can be used to assess trends in forerunner surge as a function of real-

135   time forecasted storm track parameters.

136   In Texas, we simulate surge for synthetic TCs along three tracks spaced 35 km apart and

137   making landfall in or near Galveston (Figure 1). All storms follow tracks oriented -30º clockwise

138   from north. Along the middle track (TX-T2), 42 combinations of Δp, R and V_f are simulated,

139   respectively spanning from 53 to 113 hPa, 10 to 85 km, and 3 to 12 m/s at landfall. These 42

140   simulations reveal trends consistent with those seen in the Virginia simulations, so a reduced set

141   of 19 TCs are simulated for the north (TX-T1) and south tracks (TX-T3). In all 80 unique storm

142   simulations are considered in Galveston. Results are shown for two representative locations near

143   densely populated areas, Houston (TX-1) within Galveston Bay and Galveston (TX-2) on the

144   open coast. Selected storms are simulated without Coriolis forcing in order to confirm the

145   prominent role of Ekman setup in forerunner surge generation (Figure A8).

146   **3 Results and Discussion**

147   To identify the relative influence of each storm parameter on forerunner surge, we

148   investigate correlation between the forerunner surge magnitude and storm parameters. At 12

149   hours prior to landfall, for example, partial correlation coefficients for Δp, R, and V_f are

150   respectively 0.52, 0.82, and -0.87 for Virginia, 0.71, 0.86, and -0.73 for Texas, and 0.56, 0.68,

151   and -0.83 for New York/New Jersey. As Δp and R increase, so do forerunner surge (shown

152   herein) and peak surge [19]. In contrast, while increasing V_f tends to increase peak surge

153   somewhat [23], it serves to decrease forerunner surge magnitude. This result is expected

154   considering the physics of forerunner surge demonstrated in Kennedy et al. [2] that shows strong

155   wind-generated alongshore currents on the continental shelf produce Ekman setup (ζ_{Ek}) under

156   the effect of Coriolis force. Approximated from the cross-shore momentum balance, Ekman

157   setup is:

158        $$\zeta_{Ek} = \int \frac{fU}{g}\,dx \qquad\qquad\qquad (1)$$

159   where f is the Coriolis coefficient, U is alongshore water current speed, g is gravitational

160   acceleration, and x is in the cross-shore direction. The factors controlling timing and magnitude

161   of forerunner surge are the alongshore-current speed and the cross-shore width of the current

162   (Eq. 1's integration limit).

163   Figure 2 shows simulated surge time series, where each storm is colored based on the

164 dimensional parameter $\left(\frac{R}{V_f}\right)(\Delta p)$ to reflect the positive correlation with Δp and R and negative

165 correlation with V_f. Results show that for the parameter range simulated, the forerunner surge

166 magnitude ranges from 0.0 to 2.0 m between 24 and 6 hours before landfall, in both Virginia and

167 Texas. As expected, surge increases in magnitude closer to landfall. The results further show

168 larger $\left(\frac{R}{V_f}\right)(\Delta p)$ results in larger forerunner surge. The interpretation is twofold. First, $\left(\frac{R}{V_f}\right)$

169 represents the duration in which strong cyclonic winds persist over the continental shelf. The

170 longer the wind field lingers in this relatively shallow-depth region, the more time it has to fully

171 develop an alongshore water current. Second, Δp represents overall wind-field intensity. All else

172 being equal, a more intense TC generates a more intense wind field, which in turn induces a

173 stronger alongshore current.

174   To take a step further, we use dimensional analysis to develop physical scaling laws

175 relating forerunner surge and storm track parameters near landfall. The forerunner surge

176 magnitude and timing are scaled by Δp and $\left(\frac{R}{V_f}\right)$ respectively. A region-specific characteristic

177 intensity (Δp_{char}) and characteristic duration (t_{char}) are further integrated into the scaling to

178 account for regional characteristics. Thus,

179
$$
\begin{cases}
\zeta' = \left(\frac{\gamma\zeta}{\Delta p}\right)\left(\frac{\Delta p_{char}}{\Delta p}\right)^{\alpha} & (2a) \\[2ex]
t' = \left(\frac{t}{R/V_f}\right)\left(\frac{t_{char}}{R/V_f}\right)^{\alpha} & (2b)
\end{cases}
$$

180 where γ is the specific weight of seawater, t is time before peak surge on the open coast, and ζ is

181 surge magnitude. The quantity $\left(\frac{\gamma\zeta}{\Delta p}\right)$ in Eq. 2a is derived from the momentum balance, where Δp

182 is considered proportional to surface wind stress in a quadratic form ($\Delta p \propto u_{wind}^2$) [20,24], and

183   the quantity $\left(\frac{t}{R/V_f}\right)$ in Eq. 2b represents wind duration. The term Δp_{char} is regional mean

184   observed central pressure deficit, 58 hPa in Virginia and New York/New Jersey, and 62 hPa in

185   Texas. The term t_{char} is defined as $\frac{L_{shelf}}{\sqrt{g\overline{h_{shelf}}}}$, where L_{shelf} is reference continental shelf width,

186   taken as distance from the coastline to a depth of 100 m, and $\overline{h_{shelf}}$ is reference shelf depth,

187   taken as 50 m. The term L_{shelf} represents the Ekman setup integration limit and $\sqrt{g\overline{h_{shelf}}}$

188   represents a characteristic speed of a free wave on the shelf. The best-fit coefficient α is site-

189   specific. Taken as 0 in Virginia, -0.35 in Texas, and -0.35 in New York/New Jersey, α is thought

190   to arise from the effect of a curved coastline on Ekman setup. Specifically, we hypothesize the

191   concave coastline curvatures of the Galveston and New York/New Jersey regions redirect and

192   confine the driving alongshore current, while, the Hampton Roads region's convex coastline

193   curvature has less influence on the alongshore current. After scaling, Eq.2a represents the

194   dimensionless surge (ζ') and Eq.2b represents the dimensionless timing (t') of forerunner surge.

195   By plotting the time series in this dimensionless space in Figure 3, the surge simulations at each

196   location collapse into a hyperbolic curve. Thus,

197    $$\zeta' = \frac{a}{t' + b} + c \qquad\qquad (3)$$

198   where a, b, and c are site-specific curve fitting coefficients (Table A2) that we hypothesize are

199   related to local factors, such as continental shelf width, latitude, and bathymetry.

200   Uncertainty associated with this time-evolving surge response function (Eqs. 2-3) arises

201   from two primary sources. First, these equations are based on high-fidelity synthetic storm surge

202   simulations. Thus, uncertainties related to parameterization of the wind fields, surge, and wave

203   model assumptions, are carried into the scaling. Based on comparing observations and high-

204   fidelity surge simulations for eight historical hurricanes (US Atlantic coast: Sandy [2012], Irene

205   [2011], Isabel [2003], Gloria [1985], Josephine [1984]; US Gulf of Mexico coast: Ike [2008],

206   Katrina [2005], and Rita [2005]) [25,26], this uncertainty is found to increase linearly as surge

207   magnitude increases (Figure 7). Second, uncertainty arises from the curve fitting process, and is

208   also found to scale linearly with surge magnitude (Figure 7). Thus, as a measure of uncertainty,

209   total standard deviation of the time-evolving surge response function (σ_{tot}) is:

210
$$\begin{cases} \sigma_{tot}^2 = \sigma_{model}^2 + \sigma_{function}^2 & (4a) \\ \sigma_{model}, \sigma_{function} = (k)(\zeta) + l & (4b) \end{cases}$$

211   where σ_{model} is the standard deviation of wind and surge simulations, $\sigma_{function}$ is the standard

212   deviation of surge prediction calculated by Eqs. 2-3 compared to the simulated results, ζ is

213   forerunner surge magnitude at different times, and k and l are linear regression coefficients.

214   Uncertainty in predicting the timing of forerunner arrival is also quantified as the average

215   prediction uncertainty for observed forerunner surges ranging from 0.3 to 2.0 m (Figure 8).

216   With uncertainty considered, Eqs. 2-3 may be used to rapidly predict forerunner surge for

217   a specific storm, as well as to determine the likelihood of the occurrence of storms with potential

218   to generate significant forerunner surge. As an example, Figure 5-6 shows forerunner surge at 24,

219   18, 12, and 6 hours before landfall at Virginia Beach (VA-2), Sandy Hook (NJ-2), and Galveston

220   (TX-2), where surge is calculated as ζ in Figure 5 and $\zeta \pm \sigma_{tot}$ in Figure 6 using Eqs. 2-4.

221   Within the range of storm track parameters considered, a forerunner surge of 1 m or more

222   generally occurs earlier than 12 hours before landfall. Using track parameters (Table A1), we

223   predict that 12 hours before landfall, the forerunner surge at Virginia Beach is 0.4-0.9 m during

224   Hurricane Isabel (2003), which made landfall about 200 km to the south, and is consistent with

225   an observed value of 0.5 m at the Sewells Point NOAA station ([27]; Figure A3). Hurricane

226   Sandy (2012) made landfall about 100 km to the south of Sandy Hook, where we predict the

227 forerunner surge 12 hours before landfall is 0.4-1.1 m. The observed value here was 1.2 m ([27];

228 Figure A4). We hypothesize that the slight underestimation is due to the long hovering of

229 Sandy's enormous wind field on the continental shelf before it changed direction to make

230 landfall. In Galveston, we predict Hurricane Ike's (2008) forerunner surge 24, 18, 12 and 6 hours

231 before landfall is 0.4-0.9 m, 0.5-1.1 m, 0.7-1.6 m, and 1.2-2.8 m, where observed value was

232 respectively 0.7 m, 1.1 m, 1.8 m, and 2.6 m at the Galveston Pier 21 NOAA station ([2,27];

233 Figure A6). The predicted arrival for a 1.0-m forerunner during Ike is 14±7 hours before landfall

234 (Figure S12, S13), where the observed arrival was 20 hours before landfall (Figure A6). Though

235 Hurricane Harvey's (2017) recent landfall was 250 km to the south of Galveston Pier 21, we

236 predict its forerunner surge 12 hours before landfall to be 0.4-0.9 m, while the observed value

237 was 0.5 m (Figure A7). The arrival of a 0.5-m forerunner during Harvey is predicted to be 15±7

238 hours before landfall, while the observed was 18 hours before landfall (Figure A7).

239   These prediction-observation comparisons demonstrate that Eqs. 2-4 captures the

240 predominant physical mechanisms governing forerunner surge. The slight underestimation for

241 forerunner surge during Hurricane Ike at 18 and 12 hours before landfall is expected, considering

242 the employed hydrodynamic model underestimates surge for this event during this period. This

243 prediction could be more accurate with future hydrodynamic model improvements. The overall

244 uncertainty can be reduced with improved forecasting of the spatial wind field as well as with

245 improved operational forecast storm surge models.

246   Finally, we conduct extreme value analyses using Eqs. 2-4 and existing joint probability

247 statistics in Hampton Roads [28], New York/ New Jersey, and Galveston [29,8]. To estimate 1%

248 annual exceedance probabilities (AEP) for forerunner surge, we employ the joint probability

249 method with optimal sampling (JPM-OS; [23]) achieved using time-evolving surge response

250   functions of Eqs. 2 and 3. The joint probability density function is $f =$

251    $f(R|\Delta p)f(\Delta p|x_o)f(v_f|x_o)f(x_o)$. We use published parameterized probability density functions

252   for the U.S. Gulf of Mexico [8,29] and U.S. Atlantic [28] coasts to define $f(R|\Delta p)$, $f(\Delta p|x_o)$,

253    $f(v_f|x_o)$, and $f(x_o)$, based on best available historical track information (e.g., [30,31]; A. Cox,

254   Oceanweather, Inc. personal communications). Only landfalling storms are considered, and

255   dependence on storm heading is neglected. We present uncertainty ranges based on our estimated

256   total standard deviation (Eq. 4). Results show that the 1% annual exceedance probability (AEP)

257   forerunner surge 12 hours before landfall is 0.53 ± 0.21 m at Virginia Beach, 0.71 ± 0.31 at

258   New York/ New Jersey, and 1.37 ± 0.54 m at Galveston. This preliminary probabilistic hazard

259   assessment demonstrates the Houston-Galveston area is more prone to high forerunner surge,

260   compared with Hampton Roads and New York/ New Jersey, which is expected considering the

261   much wider and shallower continental shelf, generally lower bottom friction from the muddy

262   sediments along the Texas coast, and more frequent intense storms.

263   **Summary and Conclusions**

264   Forerunner surge in advance of TC landfall can leave people stranded, preventing

265   evacuation and rescue, thus leading to greater loss of life. With projected global sea level rise

266   and projected changes in storm climatology, forerunner surge is expected to play an even more

267   critical role in coastal hazards. Thus, it is of great importance to understand what storm

268   conditions have the potential to generate large forerunner surge, and to include prediction of

269   forerunner surge in public forecasts.

270   Our results confirm Ekman setup is the leading mechanism driving forerunner surge

271   generation in surge-prone regions characterized by broad, shallow terrain. We further

272   quantitatively prove that slow-moving, large, intense storms have the most potential for

273   generating dangerous forerunner surge, because such storms generate and sustain the strong

274   alongshore currents needed to produce Ekman setup.

275   The physical scaling presented herein can be used to assess trends in forerunner surge as

276   a function of real-time forecasted storm track parameters only, allows identification of the range

277   of storm conditions in which a large forerunner surge is possible. The forecasting equations also

278   have the potential to be incorporated into coastal flooding warning systems, and may be used to

279   aid emergency managers and communities in evacuation planning and execution. Because the

280   predictive equations herein are physically based, they are also of high value to regions

281   worldwide influenced by TCs and surge threats, such as the Pacific coasts of southeast Asia,

282   west and east Australia [32], and the Bay of Bengal. In developing regions that lack sophisticated

283   computer modeling, the methods and findings can be applied directly to gauge data or limited

284   simulation results to better characterize forerunner surge threat.

285   While the TC climatology community has studied and come to consensus that future TCs

286   will be more intense under global warming [33,34], little attention has been given to the

287   influence of global warming on TC size and forward speed. Yet, such investigations are in

288   critical need given the significant influence of size and forward speed on forerunner surge.

289   Future work to improve understanding and ability to predict forerunner surge should

290   consider, for example, the influence of locally generated surge in coastal bays, tides, sea level

291   rise, and vertical flow structure (e.g, multi-layer hydrodynamic simulation) on Ekman setup.

292   **Acknowledgments**

302

References

[1] E.B. Garriott, West Indian hurricane of September 1–12, 1900, Mon. Weatther Rev. 28 (1900) 371–377.

[2] A.B. Kennedy, U. Gravois, B.C. Zachry, J.J. Westerink, M.E. Hope, J.C. Dietrich, M.D. Powell, A.T. Cox, R.A. Luettich, R.G. Dean, Origin of the Hurricane Ike forerunner surge, Geophys. Res. Lett. 38 (2011) L08608. doi:10.1029/2011GL047090.

[3] E.S. Blake, C.W. Landsea, E.J. Gibney, The deadliest, costliest, and most intense United States tropical cyclones from 1851 to 2010 (and other frequently requested hurricane facts), 2011. https://www.census.gov/history/pdf/nws-nhc-6.pdf.

[4] A. Sebastian, J. Proft, J.C. Dietrich, W. Du, P.B. Bedient, C.N. Dawson, Characterizing hurricane storm surge behavior in Galveston Bay using the SWAN + ADCIRC model, Coast. Eng. 88 (2014) 171–181. doi:10.1016/j.coastaleng.2014.03.002.

[5] A.A. Taylor, B. Glahn, Probabilistic guidance for hurricane storm surge, 19th Conf. Probab. Stat. 74 (2008).

[6] B. Glahn, A. Taylor, N. Kurkowski, W.A. Shaffer, The role of the SLOSH model in National Weather Service storm surge forecasting, Natl. Weather Dig. 33 (2009) 3–14.

[7] J.C. Dietrich, C.N. Dawson, J.M. Proft, M.T. Howard, G. Wells, J.G. Fleming, R.A. Luettich, J.J. Westerink, Z. Cobell, M. Vitse, H. Lander, B.O. Blanton, C.M. Szpilka, J.H. Atkinson, Real-Time Forecasting and Visualization of Hurricane Waves and Storm Surge Using SWAN+ADCIRC and FigureGen, in: Comput. Chall. Geosci., Springer, New York, NY, 2013: pp. 49–70. doi:10.1007/978-1-4614-7434-0_3.

[8] J.L. Irish, Y.K. Song, K.-A. Chang, Probabilistic hurricane surge forecasting using parameterized surge response functions, Geophys. Res. Lett. 38 (2011) L03606. doi:10.1029/2010GL046347.

[9] A.A. Taflanidis, A.B. Kennedy, J.J. Westerink, J. Smith, K.F. Cheung, M. Hope, S. Tanaka, Rapid assessment of wave and surge risk during landfalling hurricanes: probabilistic approach, J. Waterw. Port Coast. Ocean Eng. 139 (2013) 171–182.

[10] G. Jia, A.A. Taflanidis, N.C. Nadal-Caraballo, J.A. Melby, A.B. Kennedy, J.M. Smith, Surrogate modeling for peak or time-dependent storm surge prediction over an extended coastal region using an existing database of synthetic storms, Nat. Hazards. 81 (2016) 909–938. doi:10.1007/s11069-015-2111-1.

[11] C.W. Landsea, D.A. Glenn, W. Bredemeyer, M. Chenoweth, R. Ellis, J. Gamache, L. Hufstetler, C. Mock, R. Perez, R. Prieto, J. Sánchez-Sesma, D. Thomas, L. Woolcock, A Reanalysis of the 1911–20 Atlantic Hurricane Database, J. Clim. 21 (2008) 2138–2168. doi:10.1175/2007JCLI1119.1.

[12] R.A. Luettich, J.J. Westerink, N.W. Scheffner, ADCIRC: An Advanced Three-Dimensional Circulation Model for Shelves, Coasts, and Estuaries. Report 1. Theory and Methodology of ADCIRC-2DDI and ADCIRC-3DL. No. CERC-TR-DRP-92-6., COASTAL ENGINEERING RESEARCH CENTER VICKSBURG MS, 1992.

[13] N. Booij, L.H. Holthuijsen, R.C. Ris, The "SWAN" wave model for shallow water, Coast. Eng. Proc. 1 (1996). https://journals.tdl.org/icce/index.php/icce/article/view/5257 (accessed November 8, 2016).

[14] J.M. Smith, A.R. Sherlock, D.T. Resio, STWAVE: Steady-State Spectral Wave Model User's Manual for STWAVE, Version 3.0, 2001.

347 [15] J.C. Dietrich, Development and application of coupled hurricane wave and surge models for
348   southern Louisiana, UNIVERSITY OF NOTRE DAME, 2011.
349   http://gradworks.umi.com/34/36/3436250.html (accessed November 22, 2016).
350 [16] J.C. Dietrich, S. Tanaka, J.J. Westerink, C.N. Dawson, R.A. Luettich, M. Zijlema, L.H.
351   Holthuijsen, J.M. Smith, L.G. Westerink, H.J. Westerink, Performance of the Unstructured-
352   Mesh, SWAN+ADCIRC Model in Computing Hurricane Waves and Surge, J. Sci. Comput.
353   52 (2012) 468–497. doi:10.1007/s10915-011-9555-6.
354 [17] E.F. Thompson, V.J. Cardone, Practical Modeling of Hurricane Surface Wind Fields, J.
355   Waterw. Port Coast. Ocean Eng. 122 (1996) 195–205. doi:10.1061/(ASCE)0733-
356   950X(1996)122:4(195).
357 [18] G.J. Holland, An Analytic Model of the Wind and Pressure Profiles in Hurricanes, Mon.
358   Weather Rev. 108 (1980) 1212–1218. doi:10.1175/1520-
359   0493(1980)108<1212:AAMOTW>2.0.CO;2.
360 [19] J.L. Irish, D.T. Resio, J.J. Ratcliff, The Influence of Storm Size on Hurricane Surge, J.
361   Phys. Oceanogr. 38 (2008) 2003–2013. doi:10.1175/2008JPO3727.1.
362 [20] J.L. Irish, D.T. Resio, M.A. Cialone, A surge response function approach to coastal hazard
363   assessment. Part 2: Quantification of spatial attributes of response functions, Nat. Hazards.
364   51 (2009) 183–205. doi:10.1007/s11069-009-9381-4.
365 [21] Cialone, A.S. Grzegorzewski, D.J. Mark, M.A. Bryant, T.C. Massey, Coastal-Storm Model
366   Development and Water-Level Validation for the North Atlantic Coast Comprehensive
367   Study, J. Waterw. Port Coast. Ocean Eng. 143 (2017) 04017031.
368   doi:10.1061/(ASCE)WW.1943-5460.0000408.
369 [22] R. Berg, Tropical cyclone report: Hurricane Ike 1-14 September 2008, National Hurricane
370   Center, 2009.
371 [23] D.T. Resio, J. Irish, M. Cialone, A surge response function approach to coastal hazard
372   assessment – part 1: basic concepts, Nat. Hazards. 51 (2009) 163–182. doi:10.1007/s11069-
373   009-9379-y.
374 [24] J.L. Irish, D.T. Resio, Method for Estimating Future Hurricane Flood Probabilities and
375   Associated Uncertainty, J. Waterw. Port Coast. Ocean Eng. 139 (2013) 126–134.
376   doi:10.1061/(ASCE)WW.1943-5460.0000157.
377 [25] S. Bunya, J.C. Dietrich, J.J. Westerink, B.A. Ebersole, J.M. Smith, J.H. Atkinson, R.
378   Jensen, D.T. Resio, R.A. Luettich, C. Dawson, V.J. Cardone, A.T. Cox, M.D. Powell, H.J.
379   Westerink, H.J. Roberts, A High-Resolution Coupled Riverine Flow, Tide, Wind, Wind
380   Wave, and Storm Surge Model for Southern Louisiana and Mississippi. Part I: Model
381   Development and Validation, Mon. Weather Rev. 138 (2010) 345–377.
382   doi:10.1175/2009MWR2906.1.
383 [26] M.A. Cialone, T.C. Massey, M.E. Anderson, A.S. Grzegorzewski, R.E. Jensen, A. Cialone,
384   D.J. Mark, K.C. Pevey, B.L. Gunkel, T.O. McAlpin, North Atlantic Coast Comprehensive
385   Study (NACCS) Coastal Storm Model Simulations: Waves and Water Levels, 2015.
386 [27] NOAA, Tides and currents, (2017). https://tidesandcurrents.noaa.gov/.
387 [28] N.C. Nadal-Caraballo, J.A. Melby, V.M. Gonzalez, A.T. Cox, North Atlantic Coast
388   Comprehensive Study—Coastal Storm Hazards from Virginia to Maine, U.S. Army
389   Engineer Research and Development Center, Vicksburg, Mississippi, 2015.
390 [29] A.W. Niedoroda, D.T. Resio, G.R. Toro, D. Divoky, H.S. Das, C.W. Reed, Analysis of the
391   coastal Mississippi storm surge hazard, Ocean Eng. 37 (2010) 82–90.
392   doi:10.1016/j.oceaneng.2009.08.019.

393 [30] M.D. Powell, T.A. Reinhold, Tropical Cyclone Destructive Potential by Integrated Kinetic
394   Energy, Bull. Am. Meteorol. Soc. 88 (2007) 513–526. doi:10.1175/BAMS-88-4-513.
395 [31] C.W. Landsea, J.L. Franklin, Atlantic Hurricane Database Uncertainty and Presentation of a
396   New Database Format, Mon. Weather Rev. 141 (2013) 3576–3592. doi:10.1175/MWR-D-
397   12-00254.1.
398 [32] M. Eliot, C. Pattiaratchi, Remote forcing of water levels by tropical cyclones in southwest
399   Australia, Cont. Shelf Res. 30 (2010) 1549–1561. doi:10.1016/j.csr.2010.06.002.
400 [33] T.R. Knutson, J.L. McBride, J. Chan, K. Emanuel, G. Holland, C. Landsea, I. Held, J.P.
401   Kossin, A.K. Srivastava, M. Sugi, Tropical cyclones and climate change, Nat. Geosci. 3
402   (2010) 157–163. doi:10.1038/ngeo779.
403 [34] S. report IPCC, IPCC, 2014: Climate Change 2014: Synthesis Report. Contribution of
404   Working Groups I, II and III to the Fifth Assessment Report of the Intergovernmental Panel
405   on Climate Change, IPCC, Geneva, Switzerland, 2014. http://www.ipcc.ch/report/ar5/syr/
406   (accessed February 7, 2017).
407 [35] W.P. Stewart, Hurricane of August 16-17, 1915, 1915.
408 [36] I.M. Cline, Relation of changes in storm tides on the coast of the gulf of mexico to the
409   center and movement of hurricanes, Mon. Weather Rev. 48 (1920) 127–146.
410   doi:10.1175/1520-0493(1920)48<127:ROCIST>2.0.CO;2.
411 [37] C. Fanelli, P. Fanelli, D. Wolcott, NOAA Water Level and Meteorological Data Report—
412   Hurricane Sandy, US Department of Commerce, National Oceanic and Atmospheric
413   Administration, National Ocean Service Center for Operational Oceanographic Products
414   and Services, 2013.
415 [38] NHC, National Hurricane Center tropical cyclone advisory, (2017).
416   http://www.nhc.noaa.gov/archive/.
417 [39] RAMMB, Aircraft-based Tropical Cyclone Surface Wind Analysis, (2017).
418   http://rammb.cira.colostate.edu/products/tc_realtime/archive_sub_products.asp?product=air
419   ctcwa&storm_identifier=AL092017.
420

421   **Table 1:** Historical TCs with recorded forerunner surges. Data source: (a) Garriott [1], (b)

422   Stewart [35], (c) Kennedy et al. [2], (d) NOAA [27], (e) Cline [36], and (f) Fanelli et al. [37].

Tropical Cyclone	Area	Forerunner Surge (m) (~12 hours before landfall)
Unnamed, 1900	Galveston, TX	1.5[a]
Unnamed, 1915	Galveston, TX	2.1[b]
Ike, 2008	Galveston, TX	1.8-2.0[c][d]
Unnamed, 1915	Tampa, FL	1.5[e]
Sandy, 2012	Norfolk, VA	1.0[f]

423
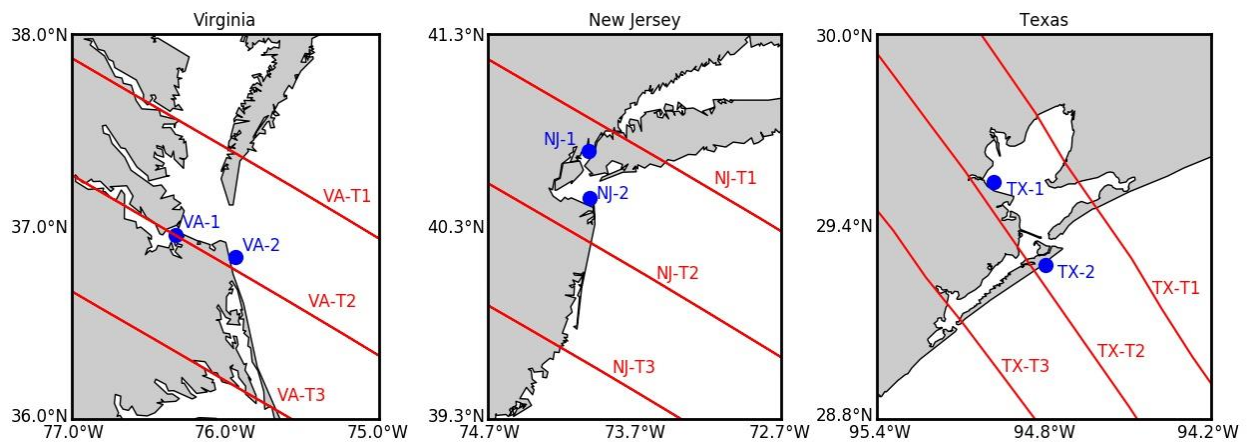
424

425   **Figure 1:** Maps of Virginia, New York/ New Jersey, and Texas coasts with synthetic TC tracks

426   and representative study locations. VA-1 and VA-2 are locations at Sewells Point and Virginia

427   Beach, respectively. TX-1 is within Galveston Bay and TX-2 is near Galveston. NJ-1 and NJ-2

428   are locations near The Battery and Sandy Hook.

429
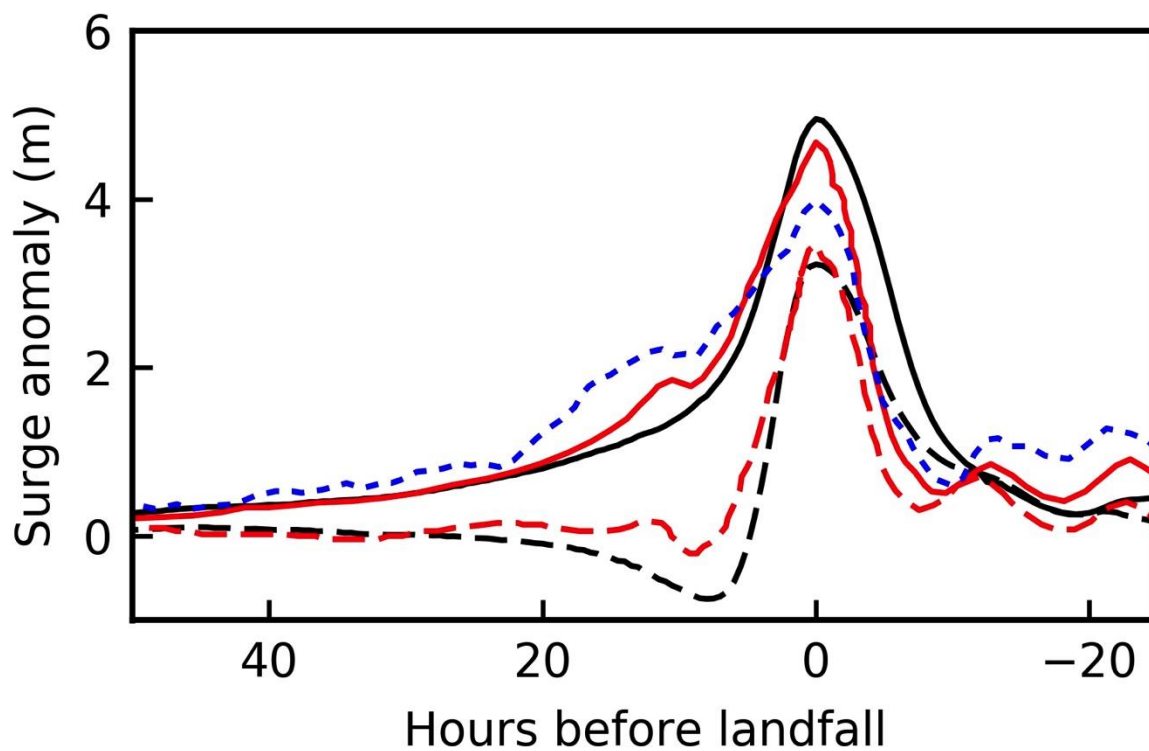
Figure 2. Surge time series validation for Hurricane Ike (2008) at location TX-2 in Figure 1. Black lines: model results with parameterized wind (PBL); red lines: model results with best reconstructed wind (H*wind); solid lines: model results with Coriollis force; dashed lines: model results without Coriollis force; dotted line: observations. Dotted and dashed lines are observations and simulations from Kennedy et al. [2].
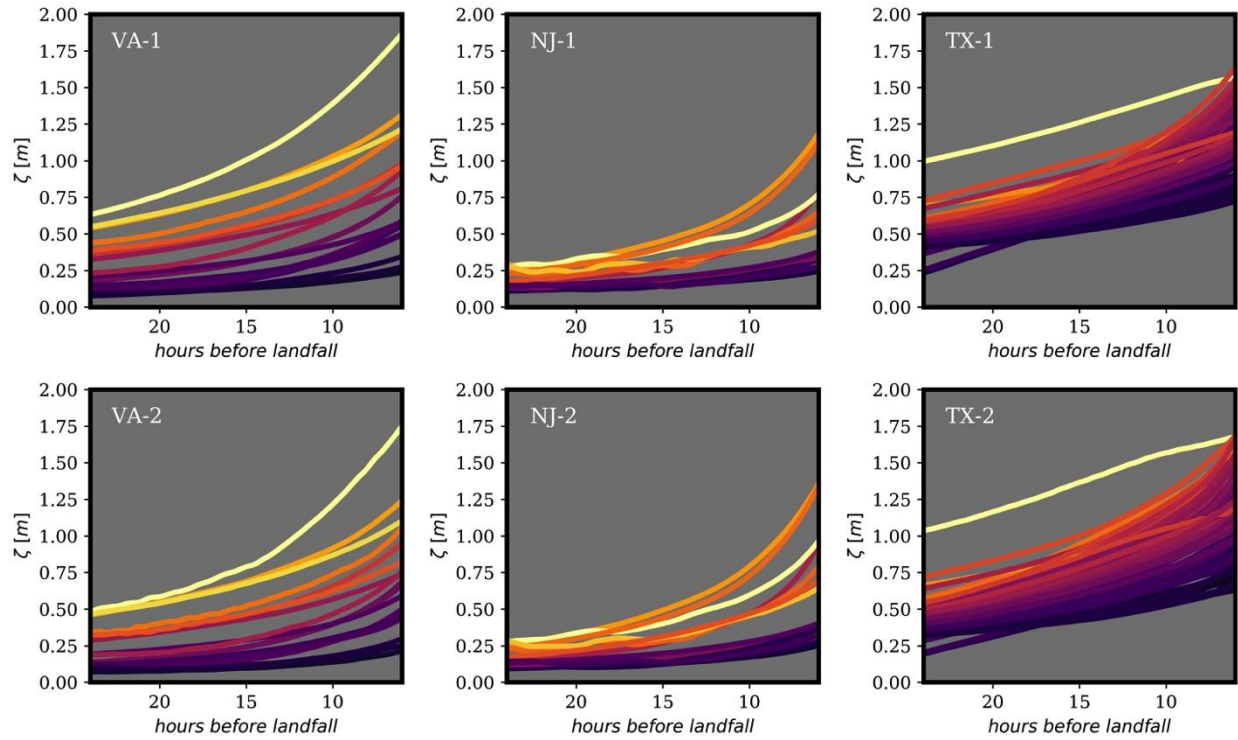
Figure 3: Surge time series of 19 simulations in Virginia, 18 simulations in New York/New Jersey and 80 simulations in Texas. Timing is defined as hours before storm landfall. Plots are colorized by $(\Delta p)\left(\frac{R}{v_f}\right)$, where lighter colors represent larger values.

439
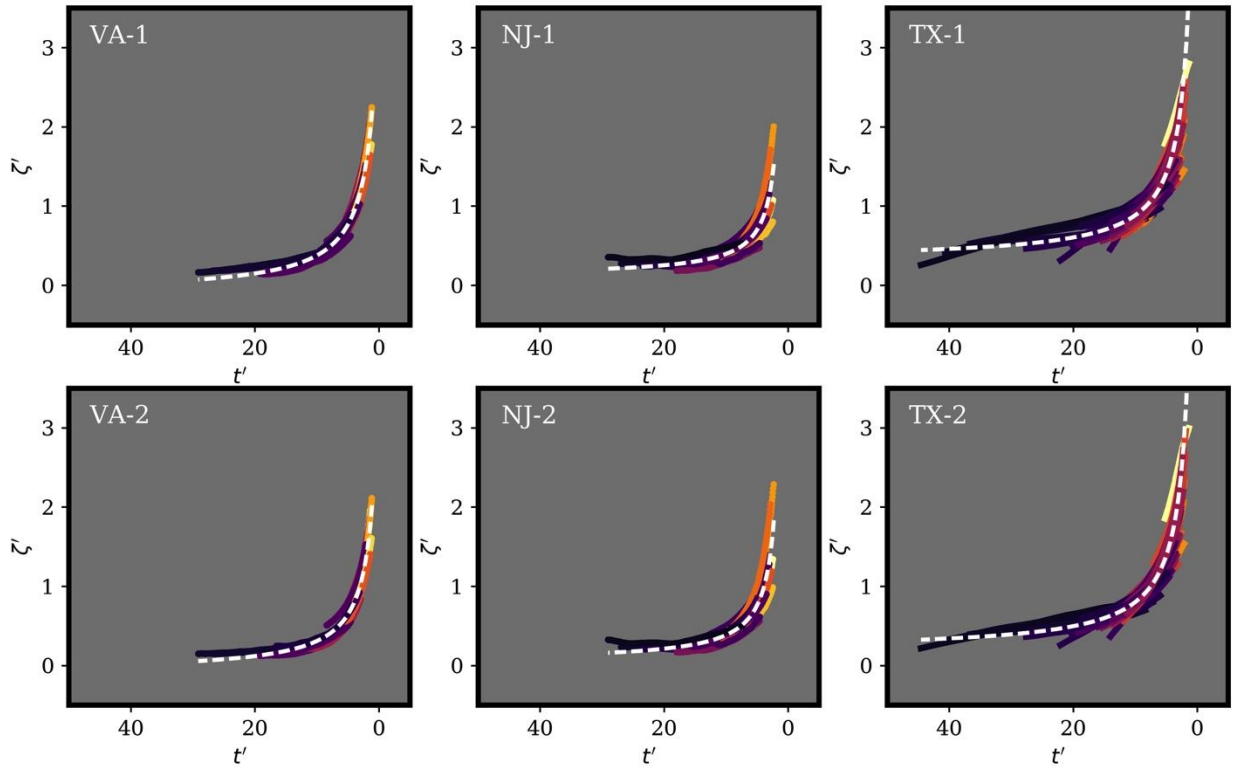
Figure 4: Plots of dimensionless surge (ζ') versus dimensionless time (t') at representative

locations. Plots are colorized by $(\Delta p)\left(\dfrac{R}{V_f}\right)$, where lighter colors represent larger values. The

dashed white lines represent fitted hyperbolic curves.

443
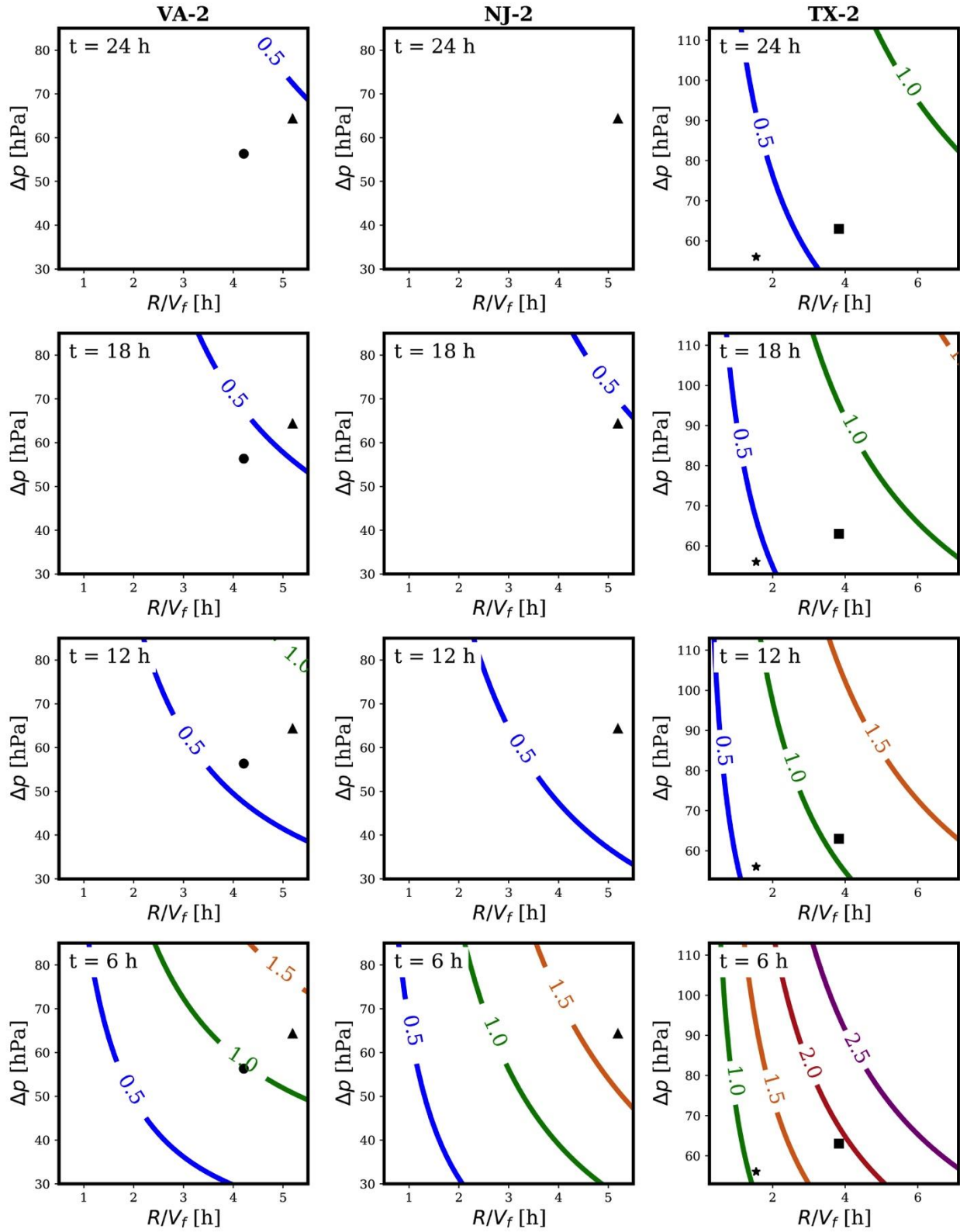
444   **Figure 5:** Deterministic forerunner surge forecasts at VA-2 (Virginia Beach) NJ-2

445   (Sandy Hook), and TX-2 (Galveston) at 24, 18, 12 and 6 hours before TC landfall, with

446   Hurricanes Isabel (2003, circles), Ike (2008, squares), Sandy (2012, triangles), and Harvey

447   (2017, stars) imposed. The 6-hr Sandy value at NJ-2 is extrapolated beyond the dimensionless

448   data limits.
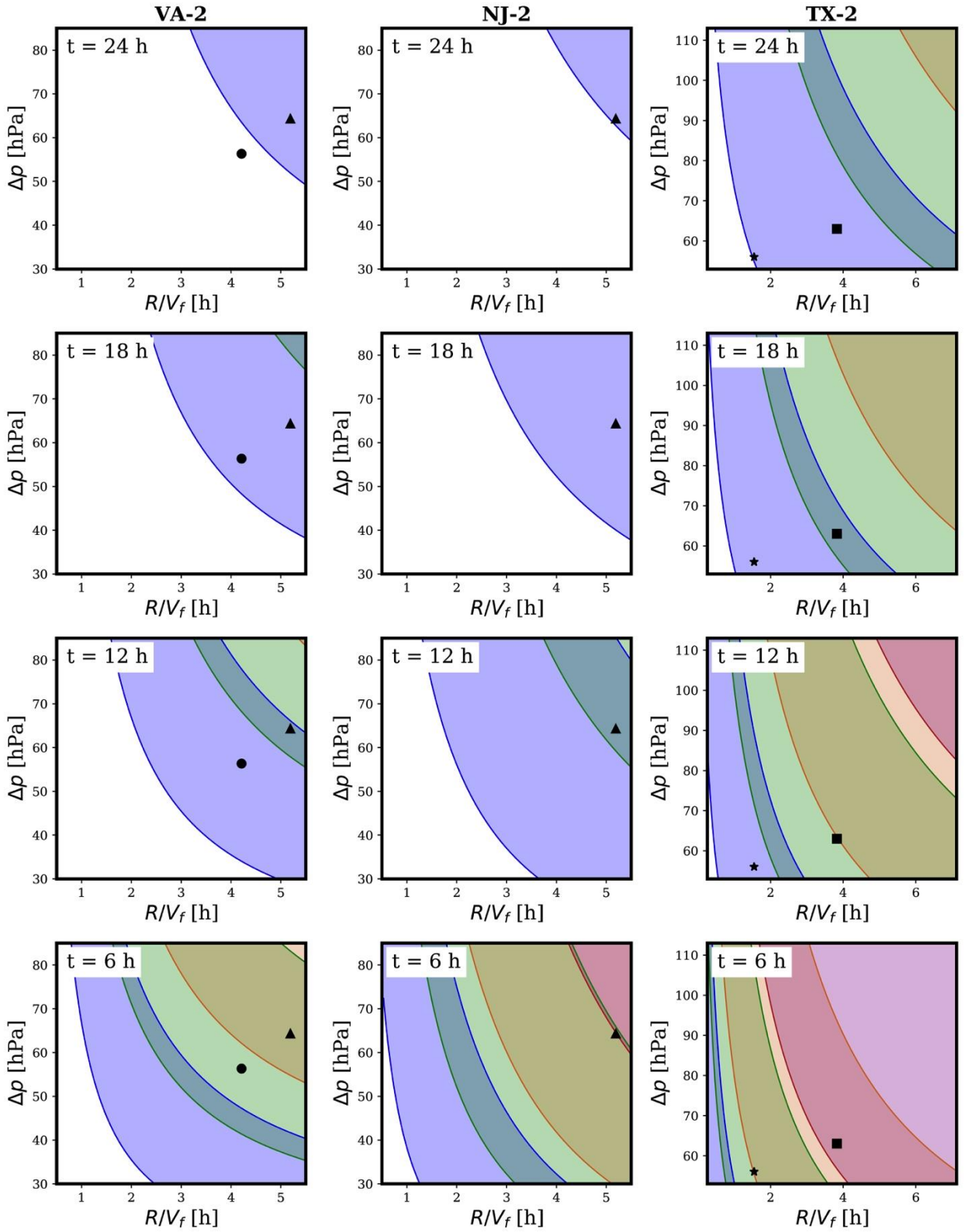
449

450

451   **Figure 6:** Forerunner surge forecasts with uncertainty bands at VA-2 (Virginia Beach)

452   NJ-2 (Sandy Hook), and TX-2 (Galveston) at 24, 18, 12 and 6 hours before TC landfall, with

453   Hurricanes Isabel (2003, circles), Ike (2008, squares), Sandy (2012, triangles), and Harvey

454   (2017, stars) imposed. Blue, green, orange and purple correspond to 0.5 m, 1.0 m, 1.5 m, and 2.5

455   m respectively. The 6-hr Sandy value at NJ-2 is extrapolated beyond the dimensionless data

456   limits.

457

VA-2
$\sigma_{model} = k \cdot \zeta + l$
$k = 0.38, \, l = 0$

$\sigma_{function} = k \cdot \zeta + l$
$k = 0.08, \, l = 0.01$

NJ-2
$\sigma_{function} = k \cdot \zeta + l$
k = 0.21, l = 0

TX-2
$\sigma_{function} = k \cdot \zeta + l$
k = 0.11, l = 0

458
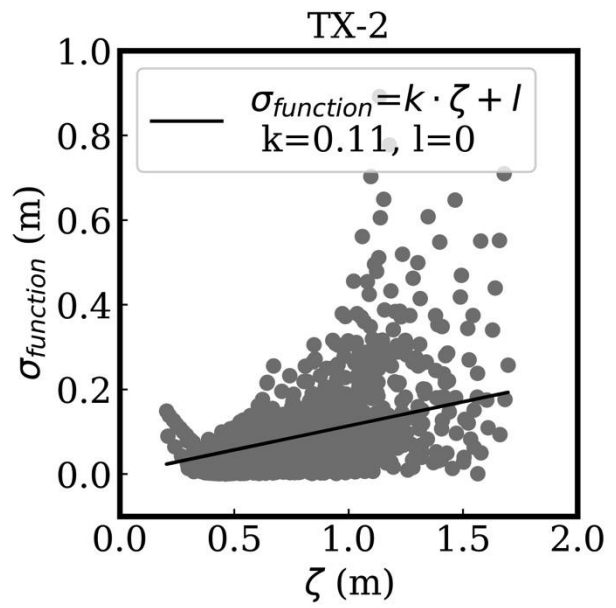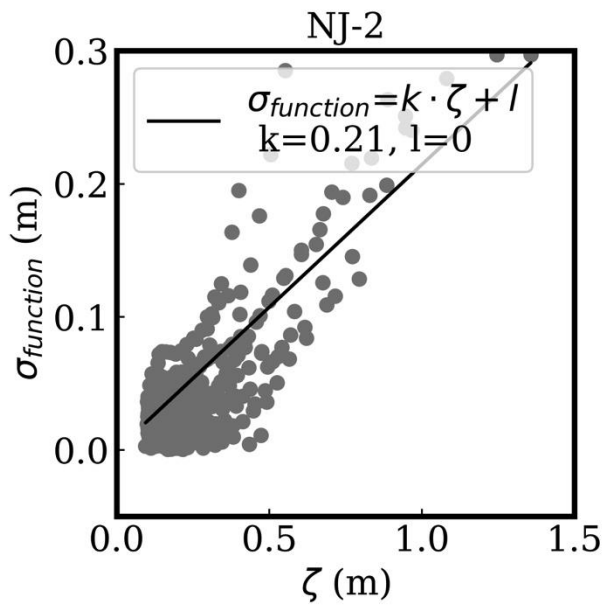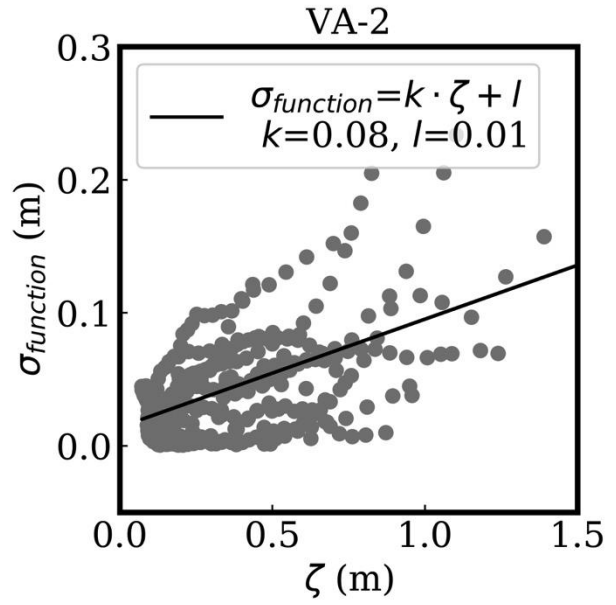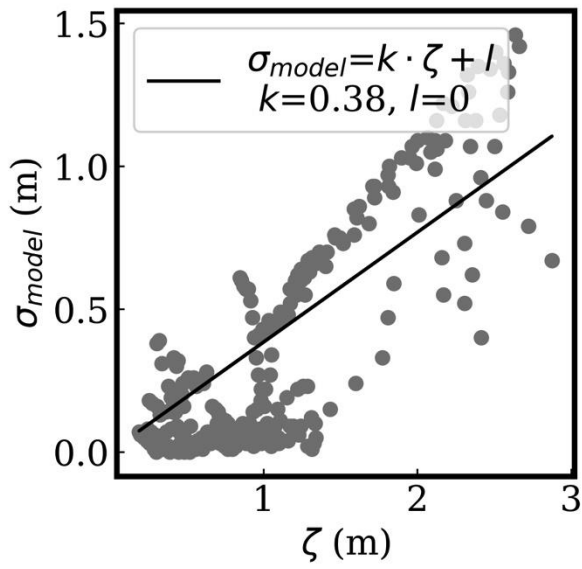
459 **Figure 7.** Surge magnitude prediction uncertainty quantification. σ_{model} is calculated as

460 simulated surge standard deviation with respect to observations [27] due to wind

461 parameterization and hydrodynamic modeling based on ADCIRC-STWAVE and ADCIRC-

462 SWAN simulations at selected coastal locations. Shown are US Atlantic Hurricanes Sandy

463 (2012), Irene (2011), Isabel (2003), Gloria (1985), Josephine (1984) [26] and US Gulf of Mexico

464 Hurricanes Ike (2008), Katrina (2005), and Rita (2005) [25,26], for surge 24 to 6 hours before

465 landfall. $\sigma_{function}$ is calculated as error in surge prediction using Eqs. 2 and 3, represented by

466 standard deviation between curve fit and surge simulations at VA-2 (Virginia Beach) NJ-2

467 (Sandy Hook), and TX-2 (Galveston), for surge 24 to 6 hours before landfall. Each gray dot

468 represents surge values averaged over a 1-hour interval.

469
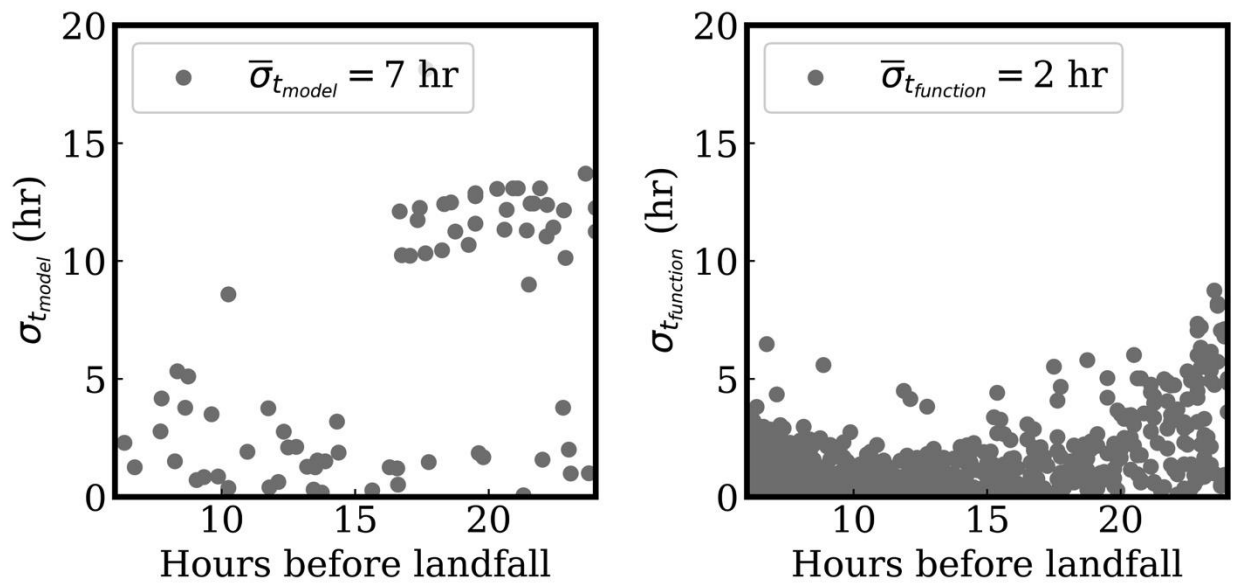
470

471   (a)   (b)

472   **Figure 8.** Surge timing prediction uncertainty quantification. (a) Simulated timing standard

473   deviation [27] due to wind parameterization and hydrodynamic modeling based on ADCIRC-

474   STWAVE and ADCIRC-SWAN simulations at selected coastal locations. Shown are US

475   Atlantic Hurricanes Sandy (2012), Irene (2011), Isabel (2003), Gloria (1985), Josephine (1984)

476   [26] and US Gulf of Mexico Hurricanes Ike (2008), Katrina (2005), and Rita (2005) [25,26], for

477   the arrival of 0.3-m to 2.0-m surge. (b) Error in timing prediction when observed forerunner

478   surge is between 0.3-m to 2.0-m using Eqs. 2 and 3.

479

480 **Appendix A**

481
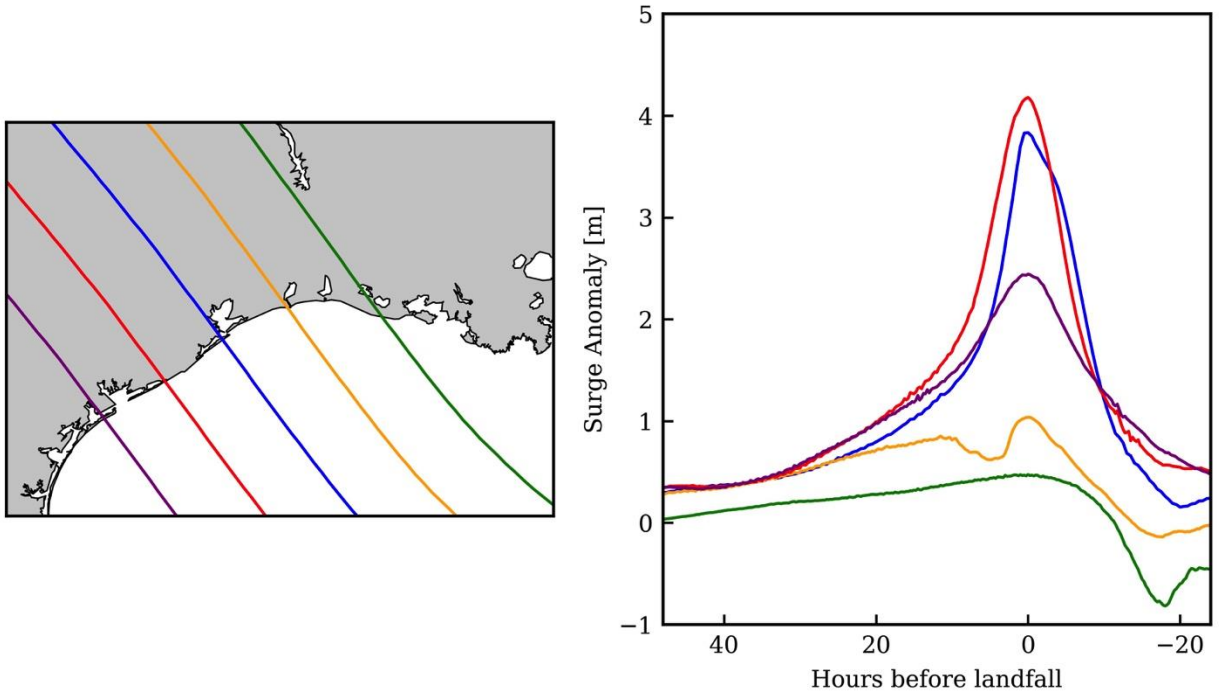
Figure A1. Tracks and surge time series for an Ike-like synthetic tropical cyclone that is shifting 100-km or 200-km to the south or north.
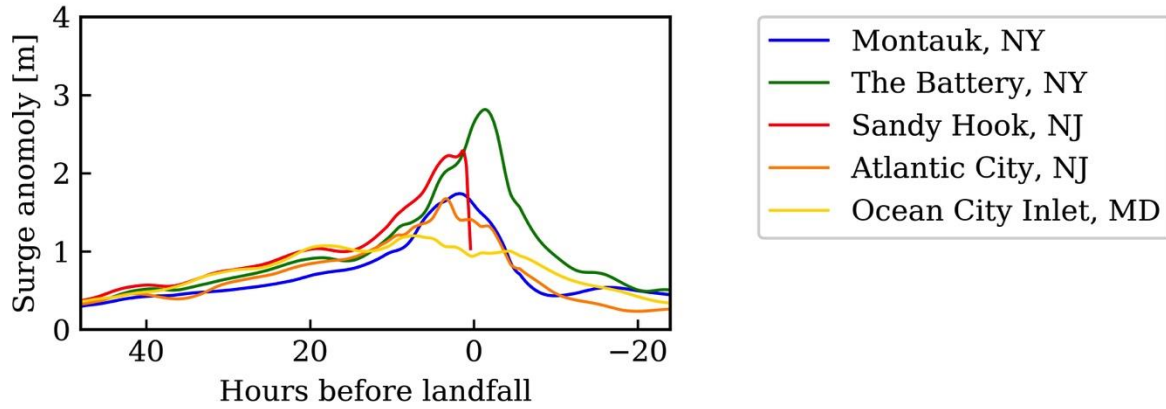
484
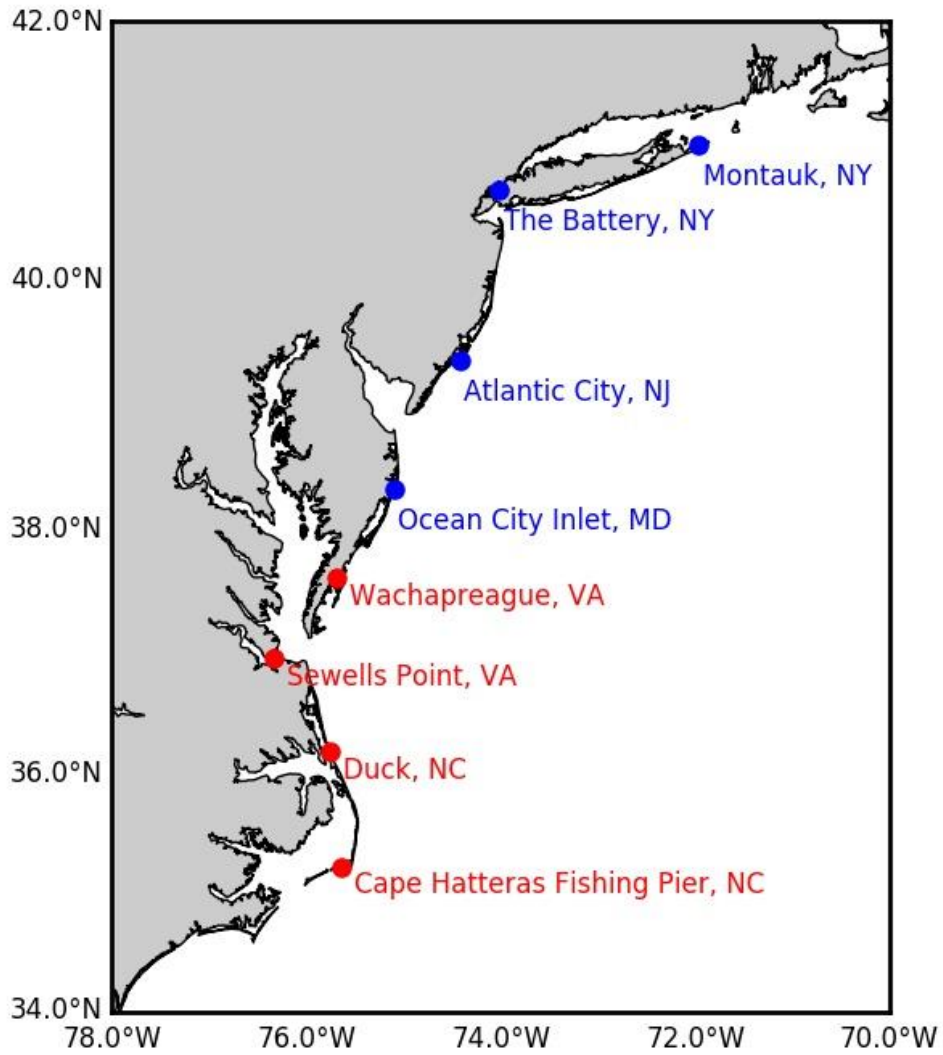
485
486 **Figure A2.** Map showing locations of NOAA (2017) observational water level data presented for
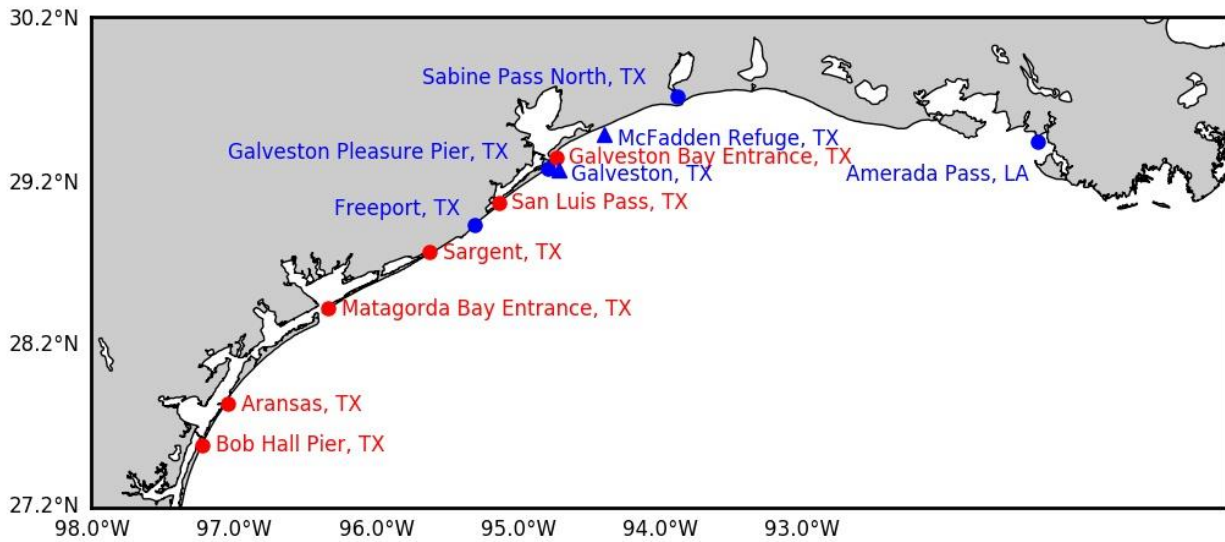487 Hurricane Sandy (2012, blue circles) and Hurricane Isabel (2003, red circles).
488
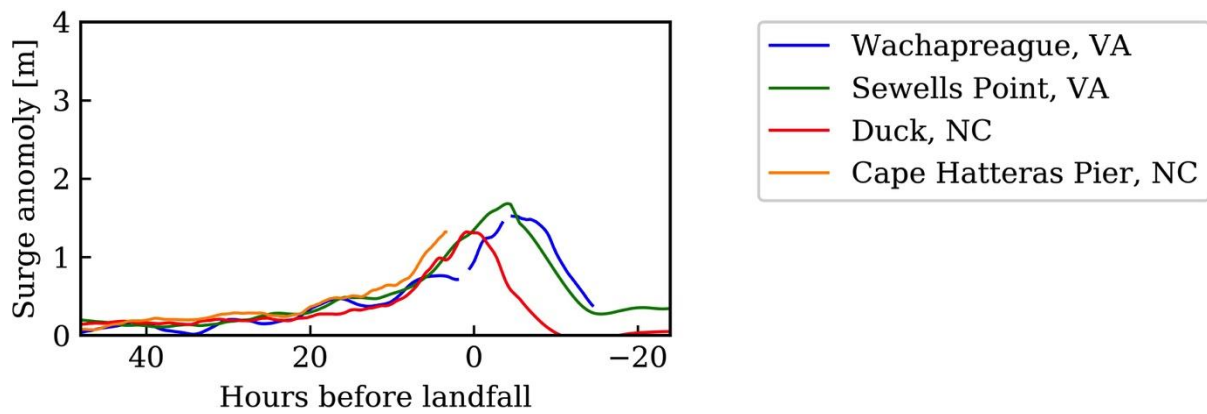
489

490   **Figure A3.** Observed water level anomaly time series (NOAA 2017) for Hurricane Isabel (2003);
491   locations shown in Figure S3.
492

493

494   **Figure A4.** Observed water level anomaly time series (NOAA 2017) for Hurricane Sandy (2012);
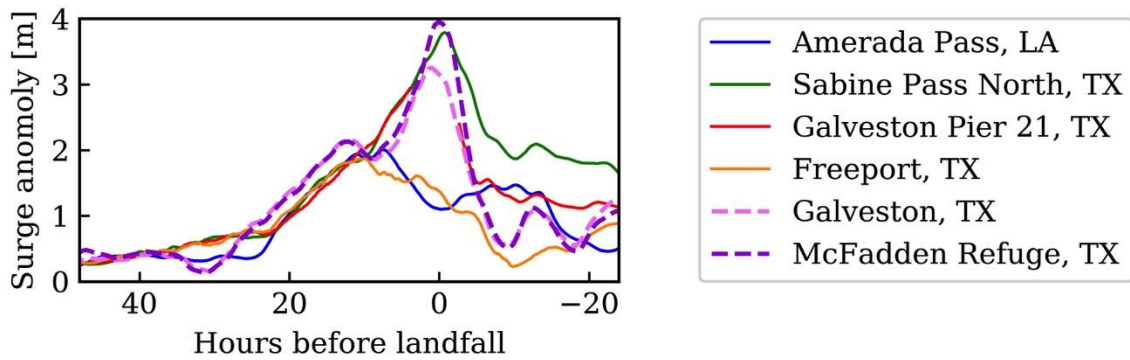495   locations shown in Figure S3.
496

497

498

Figure A5. Map showing locations of observational water level data presented for Hurricane Ike (2008, blue circles and triangles) and Hurricane Harvey (2017, red circles). NOAA (2017) stations are circles and Kennedy et al. [2] stations are triangles.
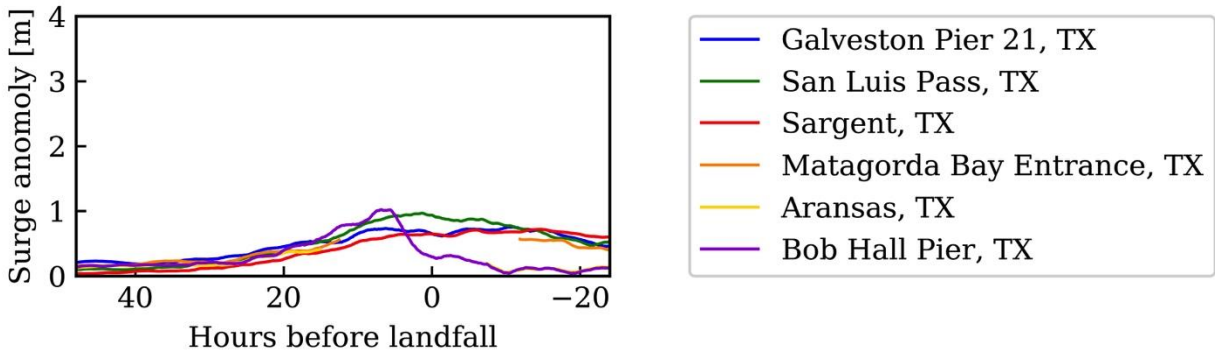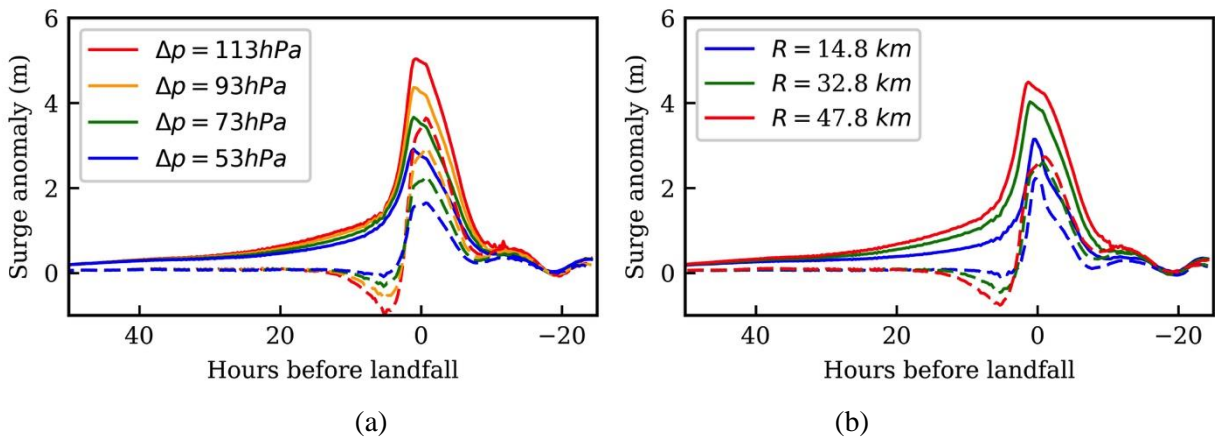
502

503

Figure A6. Observed water level anomaly time series (NOAA 2017 and Kennedy et al. 2011) for Hurricane Ike (2008); locations shown in Figure S6.

506
507

508
509　**Figure A7.** Observed water level anomaly time series (NOAA 2017) for Hurricane Harvey (2017);
510　locations shown in Figure S6.

511

512
513　　　　　　　　　　　　　　(a)　　　　　　　　　　　　　　　　　　　　　(b)

514　**Figure A8.** Simulated surge time series with (solid lines) and without (dashed lines) Coriolis forcing for
515　tropical cyclones along track TX-T2 with a 5.66 m/s V_f and (a) 32.8 km R, (b) 73 hPa Δp.

516

517

Table A1. Hurricane track parameters averaged between 6 to 24 hours before landfall. Data source: (a) NHC [38], (b) Powell and Reinhold [30], (c) Nadal-Caraballo et al. [28], (d) Sebastian et al. [4], and (e) RAMMB [39].

Hurricane	Δp (hPa)	R (km)	V_f (km/h)
Isabel (2003)	56[a]	87[b]	20[a]
Sandy (2012)	65[a]	135[c]	26[a]
Ike (2008)	63[a]	74[d]	18[a]
Harvey (2017)	56[a]	26[e]	17[a]

Table A2 Dimensionless curve fitting coefficients for Equation 3.

Location	Curve fitting coefficients		
	a	b	c
VA-1	5.44	1.24	-0.11
VA-2	4.36	0.96	-0.09
NJ-1	2.70	-0.38	0.11
NJ-2	3.21	-0.49	0.05
TX-1	5.96	0.42	0.31
TX-2	6.30	0.24	0.18

525
526